Pergamon

Int. J. Heat Mass Transfer. Vol. 38, No. 3, pp. 433–444, 1995

0017–9310/95 $9.50 + 0.00

0017–9310(94)00184–7

Theory of heat transfer-irreversible power plants—II. The optimal allocation of heat exchange equipment

ADRIAN BEJAN

Department of Mechanical Engineering and Materials Science, Duke University, Durham, NC 27708-0300, U.S.A.

(*Received* 10 *January* 1994 *and in final form* 7 *June* 1994)

Abstract—This paper shows that the power output of various power plant configurations can be maximized by properly dividing the fixed inventory of heat exchange equipment among the heat transfer components of each plant. This conclusion is built over a sequence of fundamental power-maximization problems: the solar power plant with total area constraint, the solar power plant with storage by melting, the power plant with two heat exchangers and total area constraint, the combined-cycle power plant, the power plant viewed as an insulation between its heat source and heat sink, and the power plant with by-pass heat leak to the ambient. New diagrams are reported for the power plant at maximum power, and the refrigeration plant at maximum refrigeration load.

1. INTRODUCTION

During the last two decades, entropy generation minimization emerged as a distinct subfield in heat transfer engineering. Its development was reviewed in two books [1, 2] and is not reviewed again here. The method consists of the simultaneous application of heat transfer and engineering thermodynamics principles, for the purpose of creating realistic models for heat transfer processes, devices and large-scale installations. By 'realistic' I mean models that account for the inherent irreversibility of the heat and fluid flow processes and that are always involved in the operation of such devices.

The importance of the entropy generation minimization method is stressed by the emergence of a parallel current in physics. The latter is usually traced to a 1975 paper by Curzon and Ahlborn [3] who maximized the instantaneous power output of a heat engine with heat transfer irreversibilities (finite heat exchangers) at the hot end and the cold end. According to the Gouy–Stodola theorem [1], the maximization of the power output is the same as the minimization of the rate of entropy generation of the power plant. The physics work that followed in the 1980s is commonly referred to as finite time thermodynamics [4], in which, again, the method consists of the simultaneous application of engineering thermodynamics and heat and fluid flow.

The commonality of the engineering and physics currents is further illustrated by the fact that Curzon and Ahlborn's efficiency for maximum power was reported almost two decades earlier in engineering by Novikov [5]. It is interesting that Novikov's version of power plant analysis (steady state, instead of the stroke-by-stroke analysis of Curzon and Ahlborn) became a classroom topic in engineering textbooks [6, 7], and is now the preferred analysis for demonstrating the maximum power principle (e.g. ref. [2]). Interesting also is that the model of a steady power plant with two finite heat exchangers was proposed independently in ref. [1], p. 146.

A new step in the maximization of the power from plants with heat transfer irreversibilities occurred in the first part of this study [8], where it was shown that in addition to the power maximization principle of Novikov and Curzon and Ahlborn, the power can be maximized by properly balancing the sizes of the two heat exchangers. This balance is an important thermal optimization principle, because the finiteness of the total heat exchanger inventory is a relevant constraint in the overall design of the power plant.

The objective of this second part of the study begun in ref. [8] is to examine the effect of the heat exchange inventory constraint on the thermodynamics of several fundamental configurations:

(a) the power plant with solar collector and cold-end heat exchanger;
(b) the power plant with solar collector and phase-change storage;
(c) the power plant with hot-end and cold-end heat exchangers;
(d) the combined-cycle power plant;
(e) the power plant viewed as an insulation layer between its heat source and the ambient; and
(f) the power plant with by-pass heat leak to the ambient.

This sequence is complemented by two new diagrams for illustrating the operation of a power plant at

NOMENCLATURE

A	area [m^2]
c_P	specific heat at constant pressure [J kg^{-1} K^{-1}]
C_i	internal conductance (insulation) [W K^{-1}]
$\tilde{C}_i$	dimensionless conductance, equation (54)
k_i	effective thermal conductivity [W m^{-1} K^{-1}]
L_i	thickness of internal conductance (insulation) [m]
$\dot{m}$	mass flowrate [kg s^{-1}]
q''	heat flux [W m^{-2}]
Q	heat transfer rate [W]
T	absolute temperature [K]
U	overall heat transfer coefficient [W m^{-2} K^{-1}]
W	power output [W]
$\tilde{W}$	dimensionless power output
x, y	area allocation fractions
x	distance along the internal conductance [m].

Greek symbols

α	angle, Fig. 7(a)
η	efficiency, equation (45)
η_i	efficiency, equation (52)
τ	dimensionless temperature, T/T_0.

Subscripts

c	collector
C	Carnot, or reversible compartment
H	high temperature
i	internal conductance
L	low temperature
m	melting
m	maximized once
mm	maximized twice
mmm	maximized three times
M	middle temperature
opt	optimal
out	outlet
s	from the sun
st	stagnation
0	ambient
1	high temperature cycle
2	low temperature cycle.

maximum power, and refrigeration plant at maximum refrigeration load.

2. SOLAR POWER PLANT WITH TOTAL AREA CONSTRAINT

Consider first the maximization of the power output of a plant whose working fluid is heated to T_c in a flat solar collector of area A_c. In the model of Fig. 1 the solar collector is shown separately in order to illustrate the heat loss to the ambient:

$$Q_0 = U_c A_c (T_c - T_0) \tag{1}$$

and the fact that the heat delivered to the power cycle, Q_c, is smaller than the heat absorbed from the sun, $Q_s = q'' A_c$,

$$Q_c = Q_s - Q_0. \tag{2}$$

The overall heat transfer coeffient U_c accounts for the convective heat loss to the ambient [9], or for combined convection and radiation when radiation is not the dominant heat transfer mechanism [10]. Another way of expressing the model of equations (1), (2) is [11]:

$$Q_c = Q_s \frac{T_{st} - T_c}{T_{st} - T_0} \tag{3}$$

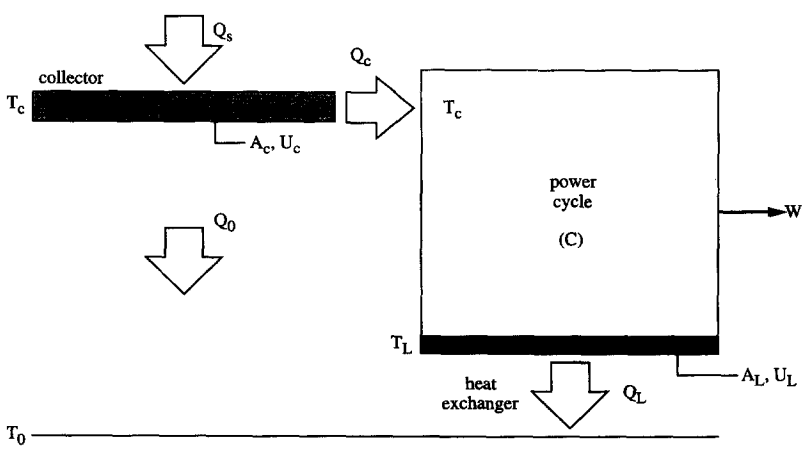

Fig. 1. Power plant model with cold-end heat exchanger and solar collector with loss of heat to the ambient.

where T_{st} is the stagnation (maximum) temperature of the collector,

$$T_{st} = T_0 + \frac{q''}{U_c} \tag{4}$$

and $q'' = Q_s/A_c$. On the right side of equation (3), the ratio $(T_{st}-T_c)/(T_{st}-T_0)$ is the collector efficiency η_c.

The right side of Fig. 1 shows the rest of the solar power plant. This consists of the cycle executed between T_c and T_L by the working fluid, and the heat exchanger between the cold end of the cycle and the ambient. We assume that the cycle is internally reversible,

$$W = Q_c - Q_L \tag{5}$$

$$\frac{Q_c}{T_c} = \frac{Q_L}{T_L}. \tag{6}$$

The heat exchanger size is described by the heat transfer area A_L and the overall heat transfer coefficient U_L. In accordance with equation (1), we assume that the heat rejected to the ambient is proportional to the driving temperature difference:

$$Q_L = U_L A_L (T_L - T_0). \tag{7}$$

Since A_c and A_L account for the physical sizes of the flat plate collector and cold-end heat exchanger, we complete the model with the size constraint:

$$A = A_c + A_L \quad \text{(constant)}. \tag{8}$$

The constraint may be expressed in terms of an area allocation fraction x,

$$A_c = (1-x)A \quad A_L = xA. \tag{9}$$

It is possible to combine equations (3) and (5)–(9) to derive the following expression for the power output,

$$\tilde{W} = \frac{U_c}{U_L}(1-x)(\tau_{st}-\tau_c) \times \left\{1 - \left[\tau_c - \frac{U_c}{U_L}\left(\frac{1}{x}-1\right)(\tau_{st}-\tau_c)\right]^{-1}\right\} \tag{10}$$

where

$$\tilde{W} = \frac{W}{U_L A T_0} \quad \tau_c = \frac{T_c}{T_0} \quad \tau_{st} = \frac{T_{st}}{T_0}. \tag{11}$$

The dimensionless power $\tilde{W}$ emerges as a function of four parameters (U_c/U_L, τ_{st}, τ_c and x), out of which τ_c and x are degrees of freedom. The collector temperature τ_c can be varied by varying the flowrate of the working fluid circulated through the collector. The fraction x varies as A_L and A_c change while the total area A remains constant.

We first maximize $\tilde{W}$ with respect to τ_c by solving $\partial\tilde{W}/\partial\tau_c = 0$. The result is the optimal collector (or engine hot end) temperature:

$$\tau_{c,opt} = \frac{\tau_{st}^{1/2} + \tau_{st}(x^{-1}-1)U_c/U_L}{1+(x^{-1}-1)U_c/U_L} \tag{12}$$

with the corresponding maximum power

$$\tilde{W}_m = \frac{x(1-x)U_c/U_L}{x+(1-x)U_c/U_L}\tau_{st}(1-\tau_{st}^{-1/2})^2. \tag{13}$$

Worth noting is that the optimal collector temperature reported in ref. [9], namely $\tau_{c,opt} = \tau_{st}^{1/2}$, agrees with the $U_c/U_L \to 0$ limit of equation (12). Indeed, in ref. [9] it was assumed that the cold end of the power cycle is in thermal equilibrium with the ambient, $T_L = T_0$, which, when A is fixed, means that U_L is infinite.

In the second step we maximize $\tilde{W}_m$ with respect to x; solving $\partial\tilde{W}/\partial x = 0$ we obtain the optimal area allocation ratio:

$$x_{opt} = \frac{1}{1+(U_L/U_c)^{1/2}}. \tag{14}$$

Substituting $x = x_{opt}$ into equation (13) we obtain the twice-maximized power output:

$$\tilde{W}_{mm} = \left[\frac{\tau_{st}^{1/2}-1}{(U_L/U_c)^{1/2}+1}\right]^2. \tag{15}$$

A more descriptive alternative to equation (14) is the optimal area ratio:

$$\left(\frac{A_L}{A_c}\right)_{opt} = \frac{x_{opt}}{1-x_{opt}} = \left(\frac{U_c}{U_L}\right)^{1/2} \tag{16}$$

which shows that when the collector is insulated well against the ambient ($U_c \ll U_L$) the optimal collector size is greater than the size of the cold-end heat exchanger of the power plant. Written as

$$U_c^{1/2} A_{c,opt} = U_L^{1/2} A_{L,opt},$$

equation (16) is qualitatively the same as the rule of the equipartition of thermal conductance inventory, $(UA)_H = (UA)_L$, which governs the maximization of power production in engines with two heat reservoirs [8], and the maximization of refrigeration load in refrigerators with two heat reservoirs [12–14].

3. SOLAR POWER PLANT WITH STORAGE BY MELTING

Consider now the proposal to store temporarily the collected solar energy by melting a phase-change material. As shown in Fig. 2, this can be accomplished by heating a stream ($\dot{m}$) inside the collector, and using this stream to melt a material at the melting point T_m. The surface of the melting material is A_m and the heat transfer coefficient based on A_m is U_m. As in refs. [15–17], we assume that above the melting material the hot stream is well mixed at the outlet temperature T_{out}. The collector model continues to be described by equations (1)–(4).

It was shown in ref. [17] that the simplest way to evaluate the potential power output associated with melting a certain amount of material at T_m is by con-

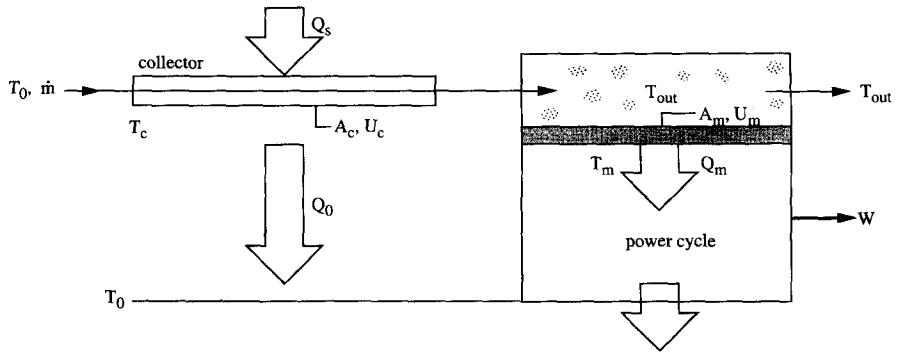

Fig. 2. Power plant model with solar collector and energy storage by melting.

sidering the internally reversible power cycle drawn under the A_m surface in Fig. 2. The steady state prevails when the heat input to the power cycle (Q_m) matches the heat transferred from the hot fluid (T_{out}) to the melting surface (T_m):

$$Q_m = \dot{m}c_P(T_c - T_{out}) = U_m A_m(T_{out} - T_m). \quad (17)$$

The heat input Q_m and the instantaneous power output $W = Q_m(1 - T_0/T_m)$ can be estimated by eliminating T_{out} between equations (17). The result is:

$$W = \frac{U_m A_m}{1 + U_m A_m/(\dot{m}c_P)}(T_c - T_m)\left(1 - \frac{T_0}{T_m}\right). \quad (18)$$

Maximizing W with respect to T_m we find:

$$T_{m,opt} = (T_0 T_c)^{1/2} \quad (19)$$

$$W_m = \frac{U_m A_m T_c(1 - \tau_c^{-1/2})^2}{1 + U_m A_m/(\dot{m}c_P)}. \quad (20)$$

The optimal melting temperature of equation (19) agrees with the conclusions reached in studies focussed specifically on the phase-change storage process [18, 19]. There are two new aspects to consider in the present problem: the collector temperature can vary in accordance with the flowrate,

$$Q_s = \dot{m}c_P(T_c - T_0) + U_c A_c(T_c - T_0) \quad (21)$$

and the total heat transfer area is constrained,

$$A = A_c + A_m \quad \text{(constant)} \quad (22)$$

or

$$A_c = (1 - y)A \quad A_m = yA. \quad (23)$$

Combining equation (20) with equations (4), (21) and (23), we rewrite the once-maximized power output as

$$\tilde{W}_m = \frac{W_m}{U_c A T_0} = \frac{(\tau_{st} - \tau_c)(\tau_c^{1/2} - 1)^2}{\dfrac{\tau_c - 1}{1 - y} + \dfrac{\tau_{st} - \tau_c}{yU_m/U_c}}. \quad (24)$$

This expression can be maximized again, this time with respect to y and the results are

$$\left(\frac{A_c}{A_m}\right)_{opt} = \frac{1 - y_{opt}}{y_{opt}} = \left(\frac{\tau_c - 1}{\tau_{st} - \tau_c} \cdot \frac{U_m}{U_c}\right)^{1/2} \quad (25)$$

$$\tilde{W}_{mm} = \frac{(\tau_{st} - \tau_c)(\tau_c^{1/2} - 1)^2}{[(\tau_c - 1)^{1/2} + (U_c/U_m)^{1/2}(\tau_{st} - \tau_c)^{1/2}]^2}. \quad (26)$$

Finally, the $\tilde{W}_{mm}$ expression can be maximized numerically with respect to the collector temperature τ_c. As shown at the bottom of Fig. 3, the optimal collector temperature depends on τ_{st} and the ratio U_c/U_m: however, the U_c/U_m effect is weak. The effect of the stagnation temperature is stronger and, as an approximation, $\tau_{c,opt}$ varies as $\tau_{st}^{1/2}$. This last feature agrees with the conclusion reached in ref. [9] where the collector was coupled with a reversible power cycle. The upper portion of Fig. 3 shows the corresponding power output, which has been maximized three times, $\tilde{W}_{mmm}$. The power output increases as the stagnation temperature increases and as the collector heat loss coefficient decreases.

Substituting $\tau_c = \tau_{c,opt}$ into equations (25) and (26) we obtain the optimal area allocation fraction shown in Fig. 4. The heat transfer coefficient ratio has a noticeable effect, while the effect of the stagnation temperature is negligible. The figure shows that more area should be allocated to the collector when the

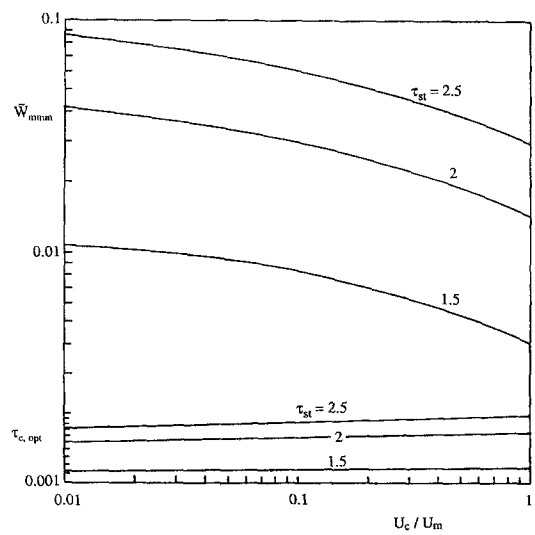

Fig. 3. The optimal collector temperature and the maximum power associated with storing solar heating by melting.

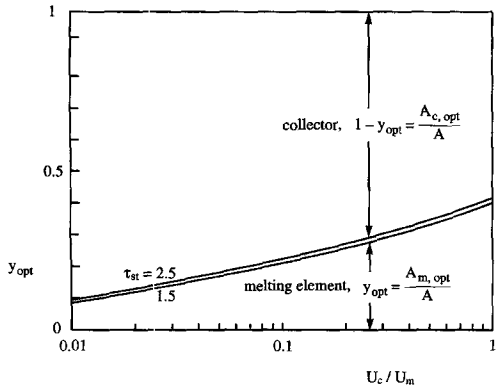

Fig. 4. The optimal allocation of heat transfer area for the phase-change storage of solar energy.

collector heat loss coefficient U_c decreases relative to U_m. It is worth noting that the $y_{opt}(\tau_{st}, U_c/U_m)$ curves do not agree with the 'rule of thumb' that may be inferred (wrongly) from ref. [8], according to which the optimum is characterized by thermal conductances of equal size. In the present case, equal thermal conductances means $U_cA_c = U_mA_m$, or $y = (1+U_m/U_c)^{-1}$, which agrees only qualitatively with the y_{opt} curves plotted in Fig. 4.

4. POWER PLANT WITH TOTAL AREA CONSTRAINT

The observation made in the preceeding paragraph raises a question concerning the equipartition of the thermal conductance inventory, when, as the optimization rule found in ref. [8],

$$(U_HA_H)_{opt} = (U_LA_L)_{opt} = \frac{1}{2}UA. \tag{27}$$

This rule is based on the power plant model of Fig. 5 and the assumption that the total thermal conductance is constrained,

$$UA = U_HA_H + U_LA_L \quad \text{(constant)}. \tag{28}$$

The power plant operates between T_H and T_L, and has three sources of irreversibility: the hot-end heat exchanger, $Q_H = U_HA_H(T_H - T_{HC})$, the cold-end heat exchanger, $Q_L = U_LA_L(T_{LC} - T_L)$, and the internal heat leak through the power plant, form T_H to T_L, namely $Q_i = C_i(T_H - T_L)$, where C_i is the thermal conductance of the power plant as an insulation between T_H and T_L. The pieces of hardware that contribute to C_i are reviewed in ref. [8].

The question we consider in this section is whether the design rule (27) changes if the thermal conductance constraint (28) is replaced by a constraint of type (8) and (22), namely the total area constraint:

$$A = A_H + A_L \quad \text{(constant)}. \tag{29}$$

By repeating the analysis detailed in ref. [8], it is easy to show that the power output of the plant is maximized when:

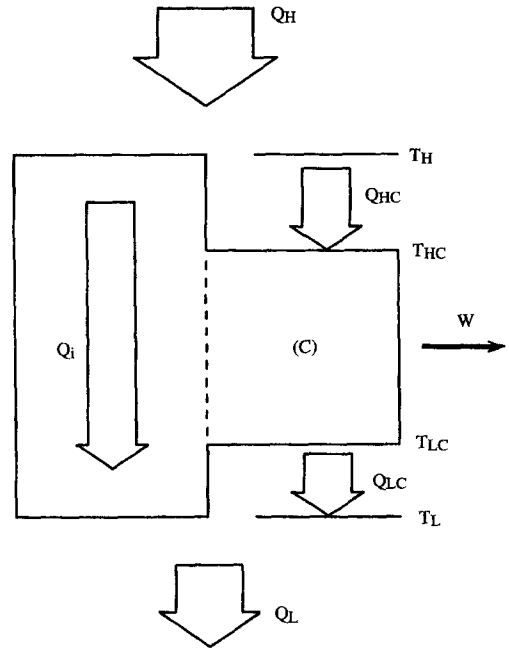

Fig. 5. Power plant model with three sources of irreversibility [8].

$$\frac{A_{H,opt}}{A} = \left[1+\left(\frac{U_H}{U_L}\right)^{1/2}\right]^{-1} \quad (A = \text{constant}). \tag{30}$$

Equation (30) is shown with solid line in Fig. 6. We see that a larger fraction of the area supply should be allocated to the heat exchanger whose overall heat transfer coefficient is lower.

It is interesting to compare this last conclusion with the optimal design based on constant UA. Equation (27) is the same as:

$$\frac{A_{H,opt}}{A} = \left(1+\frac{U_H}{U_L}\right)^{-1} \quad (UA = \text{constant}) \tag{31}$$

which is shown with dashed line in Fig. 6. The new conclusion made visible by Fig. 6 is that the optimal

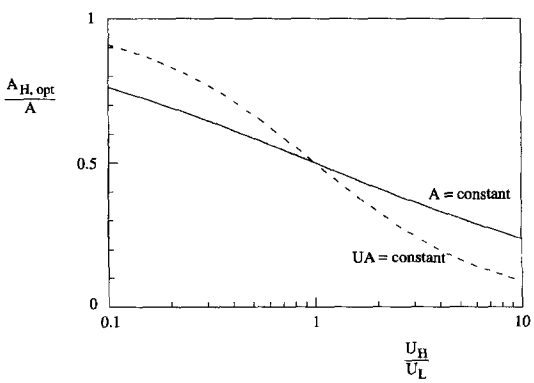

Fig. 6. The effect of the heat exchanger inventory constraint (UA vs A) on the optimal allocation of heat transfer area between the two heat exchangers of the power plant of Fig. 5.

area allocation ratio for fixed UA is qualitatively the same as the ratio recommended when A is fixed. Relative to the A constraint, however, the use of the UA constraint tends to exaggerate the inequality between $A_{H,opt}$ and $A_{L,opt}$.

It is worth pursuing the A constraint one step further. It can be shown that the twice maximized power output that corresponds to the optimal area allocation ratio (30) and the optimal temperature ratio of Novikov, Curzon and Ahlborn, $(T_{HC}/T_{LC})_{opt} = (T_H/T_L)^{1/2}$, is

$$W_{mm} = \frac{U_H U_L A T_L}{(U_H^{1/2} + U_L^{1/2})^2}\left[\left(\frac{T_H}{T_L}\right)^{1/2} - 1\right]^2. \quad (32)$$

Let us suppose that we have the means to augment only one of the heat transfer processes (U_H or U_L) by a certain small increment ε, such that the augmented coefficient is $(1+\varepsilon)U_H$ instead of U_H, or $(1+\varepsilon)U_L$ instead of U_L. The question is *where* should we direct the augmentation effort and investment, at the hot end or at the cold end [1]?

Consider the two alternatives. First, we replace U_H by $(1+\varepsilon)U_H$ in equation (32), and obtain a new power output that we label W_H. Second, if we substitute $(1+\varepsilon)U_L$ in place of U_L in equation (32) we obtain another power output, W_L. Dividing the two results, and invoking the limit $\varepsilon \to 0$ we obtain:

$$\frac{W_H}{W_L} \cong 1 + \frac{1-(U_H/U_L)^{1/2}}{1+(U_H/U_L)^{1/2}}\varepsilon \quad (33)$$

which shows that $W_H > W_L$ when $U_H < U_L$, and that $W_H < W_L$ when $U_H > U_L$. We conclude that the augmentation effort must always be directed at the heat exchanger with the lower heat transfer coefficient.

5. GRAPHIC REPRESENTATION OF THE OPTIMAL ALLOCATION OF HEAT EXCHANGE EQUIPMENT FOR MAXIMUM POWER

At this point a description of a new diagram that illustrates the functioning of the power plant of Fig. 5 under maximum power conditions will be given. Figure 7(a) was reported in ref. [8], where it was shown that, if the power output is maximized with respect to (i) the temperature ratio of the inner (reversible) compartment, i.e. $T_{HC}/T_{LC} = (T_H/T_L)^{1/2}$, *and* (ii) the allocation of thermal conductance, i.e. equation (27), the four temperatures (T_H, T_{HC}, T_{LC}, T_L) are such that:

$$\frac{T_H - T_{HC}}{T_{HC}} = \frac{T_{LC} - T_L}{T_{LC}} = \tan\alpha. \quad (34)$$

The angle α is an important parameter that depends only on the overall temperature ratio of the power plant,

$$\tan\alpha = \frac{1-(T_L/T_H)^{1/2}}{1+(T_L/T_H)^{1/2}}. \quad (35)$$

Note further that $\tan\alpha = \eta/(2-\eta)$, where η is the efficiency of the twice optimized power plant, $\eta = 1-(T_L/T_H)^{1/2}$.

New in Fig. 7 are the second and third drawings, which show the flow and augmentation of entropy as the entropy flows through the power plant. These drawings correspond to the limit $C_i \to 0$, where the irreversibility of the power plant of Fig. 5 is due almost entirely to the two heat exchangers. The abscissas of these new drawings show the entropy transfer rate Q/T as it progresses toward lower temperatures through the engine.

Figure 7(b) shows that the Q/T stream starts as Q_H/T_H as it enters the power plant at T_H. It is then augmented by an amount dictated by the angle α, as it flows across the first heat exchanger. Across the inner compartment, the entropy stream remains unchanged, $Q_H/T_{HC} = Q_L/T_{LC}$. Finally, across the second heat exchanger, the entropy stream is augmented again by the irreversibility of the transfer of Q_L from T_{LC} to T_L. This second augmentation too is dictated by α.

The analysis that stands behind the construction of Fig. 7(b) is omitted for the sake of brevity. The analytical version of this figure can be deduced from the drawing, for example by noting that $Q_H/T_{HC} = (Q_H/T_H)(1+\tan\alpha)$. The construction of Fig. 7(b) begins from the top of the drawing, by selecting the unit horizontal length Q_H/T_H. The construction progresses downward in the direction indicated by the arrows. The construction ends at point M: note that point P must be selected on the horizontal line such that the arc NM meets the line RM at M.

Figure 7(c) is a symmetric version of the entropy stream constructed graphically in Fig. 7(b). The contribution of Fig. 7(b) and (c) is to show that the power plant is a system through which entropy flows from the hot end to the cold end. The entropy stream increases as it traverses the heat exchangers: however, the larger of the two increases occurs across the cold-end heat exchanger. This is somewhat unexpected, because the cold-end heat exchanger has the smaller temperature difference ($T_{LC} - T_L < T_H - T_{HC}$) and the smaller heat transfer rate ($Q_L < Q_H$).

6. GRAPHIC REPRESENTATION OF THE OPTIMAL ALLOCATION OF HEAT EXCHANGE EQUIPMENT FOR MAXIMUM REFRIGERATION

Consider briefly the corresponding entropy stream diagram for a refrigeration plant that operates between the load level T_L and ambient T_H. According to the model used in refs. [12] and [14], the irreversibility is due to the two heat exchangers, $Q_L = U_L A_L(T_L - T_{LC})$ and $Q_H = U_H A_H(T_{HC} - T_H)$, where Q_L and Q_H are the refrigeration load and the heat rejected to the ambient. It was shown [12, 14] that when the total thermal conductance inventory is constrained, cf. equation (28), the refrigeration load is maximized

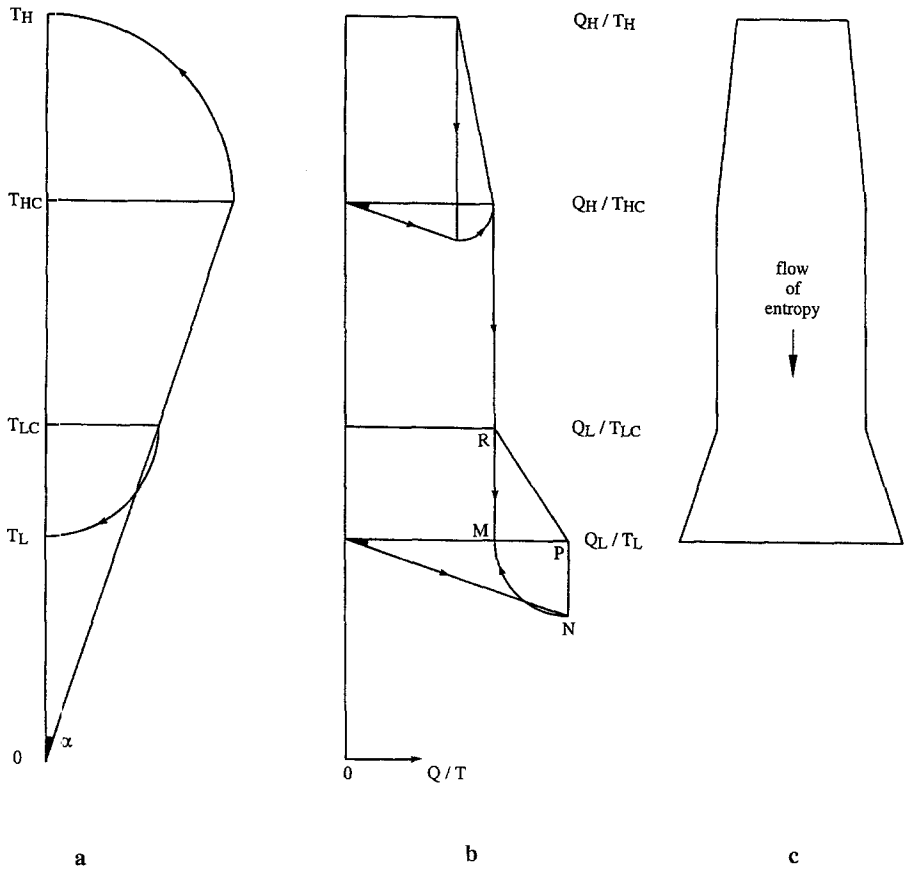

Fig. 7. The flow and growth of the entropy stream through a power plant operating at maximum power output.

if the thermal conductance is divided evenly between the two heat exchangers, cf. equation (27). This optimization rule is the basis for Fig. 8(a), which is reported here for the first time. This figure shows the positions of T_{HC}, T_H, T_L and T_{LC} on the absolute temperature scale such that $(T_{HC}-T_H)/T_{HC} = (T_L-T_{LC})/T_{LC}$.

Figure 8(b) illustrates step-by-step the evolution of the entropy stream as it flows and grows through the refrigeration plant. The construction begins with the unit length Q_L/T_L drawn horizontally at the level T_L. It ends at point M. The entropy stream experiences its first increase through the cold-end heat exchanger. It then flows upward, and at constant strength, from T_{LC} to T_{HC}. It experiences a second and larger increase through the hot-end heat exchanger. The entropy stream was redrawn in Fig. 8 as a ribbon that is bent twice, at T_{LC} and T_{HC}. Again, the stream starts at T_L, and arrives significantly larger at T_H. The entropy stream flows upward (i.e. toward higher temperatures) through the reversible compartment of the refrigeration plant, and downward through irreversible compartments (the two heat exchangers).

7. COMBINED-CYCLE POWER PLANT

Now we focus on another interesting extension of the double maximization of the power output encountered in the study of Fig. 5. That power plant model is repeated in Fig. 9(a), where it is assumed that the internal conductance irreversibility is negligible ($C_i = 0$). The question we address is how to maximize the total power output of a combined-cycle power plant that operates between the same temperatures (T_H, T_L) and uses the same heat exchange inventory as the original plant. In the combined-cycle power plant of Fig. 9(b) there are three heat exchangers,

$$UA = U_H A_H + U_M A_M + U_L A_L \quad \text{(constant)} \qquad (36)$$

and two internally reversible compartments, the high temperature cycle between T_{H1} and T_{L1}, and the low temperature cycle between T_{H2} and T_{L2}.

The optimization of the power plant cascade of Fig. 9(a) was also considered by Rubin and Andresen [20]. The new aspect considered in this section is the UA constraint (36), and the optimal allocation of the UA inventory between the three heat exchangers.

This problem can be solved analytically in two steps. In the first step we assume that the temperature level T_{L1} is fixed, and then we maximize W_1 and W_2. The analysis in this first step is the same as in refs. [2, 5–8]: therefore we can omit the details. For the part contained between T_H and T_{L1} we find that the optimal T_{H1} temperature is:

$$T_{H1,opt} = (T_H T_{L1})^{1/2} \qquad (37)$$

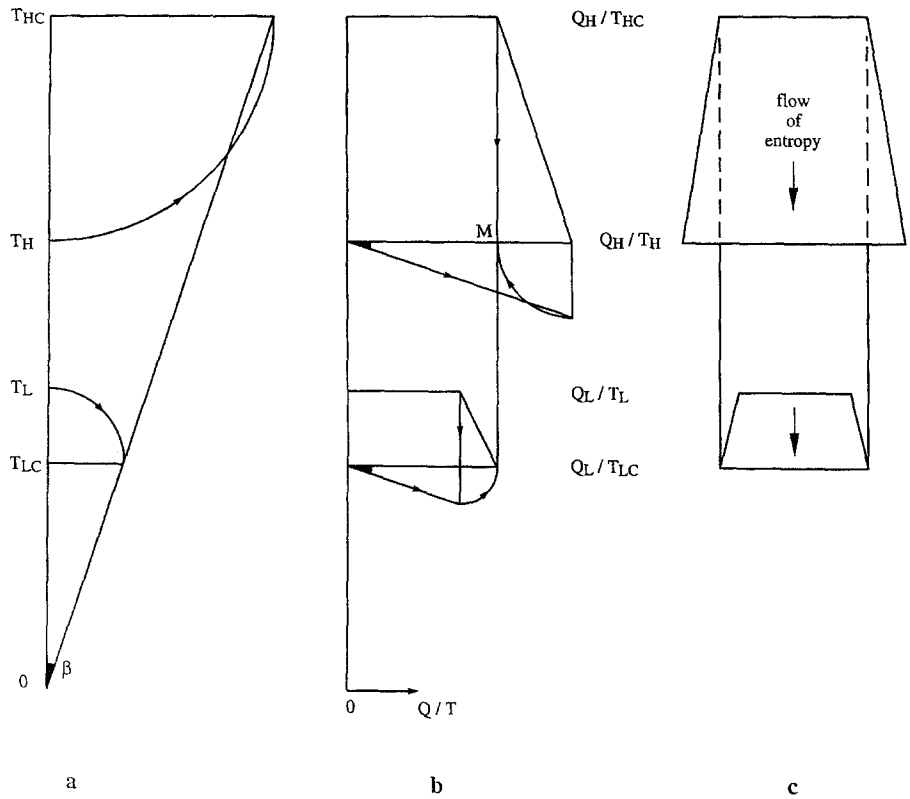

Fig. 8. The flow and growth of the entropy stream through a refrigeration plant operating at maximum refrigeration load.

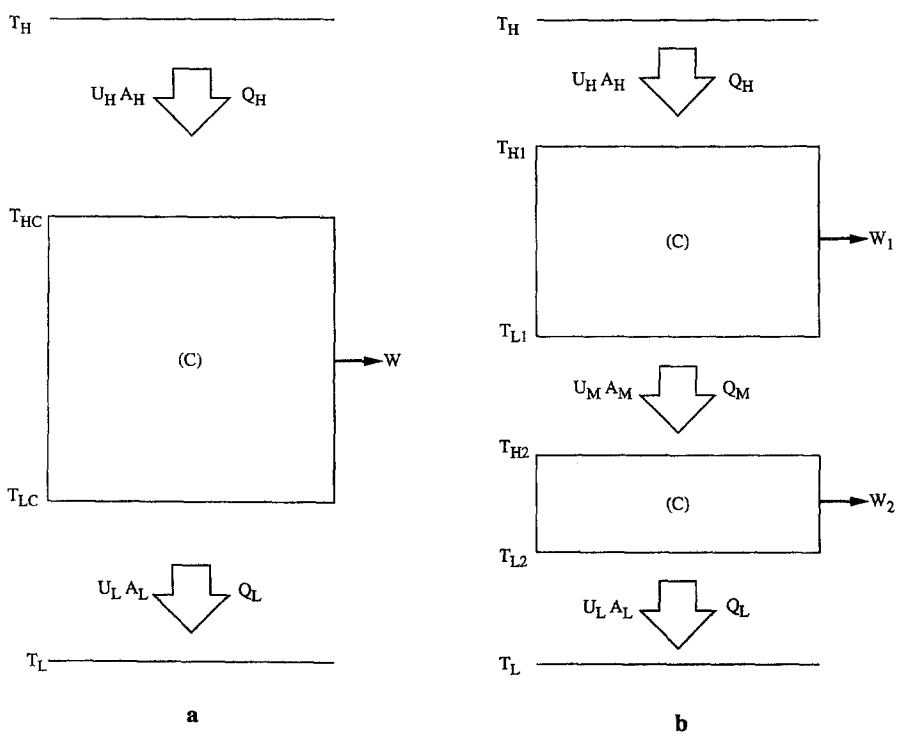

Fig. 9. (a) Power plant with two heat exchangers. (b) Combined-cycle power plant with three heat exchangers.

and that the corresponding maximum power output of the upper cycle is:

$$W_1 = U_H A_H T_H \left[1 - \left(\frac{T_{L1}}{T_H}\right)^{1/2}\right]^2. \quad (38)$$

For the part contained between T_{L1} and T_L the optimization rules are known from refs. [3, 5], namely $(T_{H2}/T_{L2})_{opt} = (T_{L1}/T_L)^{1/2}$, and from refs. [2, 8], specifically $U_M A_M = U_L A_L$. The corresponding maximum power output of the lower cycle is:

$$W_2 = \tfrac{1}{2} U_L A_L T_{L1} \left[1 - \left(\frac{T_L}{T_{L1}}\right)^{1/2}\right]^2. \quad (39)$$

In the second step of the analysis we pursue the maximization of the sum $W_1 + W_2$ with respect to two parameters, T_{L1} and the relative size of $U_L A_L$. By adding equations (38) and (39) we obtain:

$$\frac{W_1 + W_2}{U_H A_H T_H} = \left[1 - \left(\frac{T_{L1}}{T_H}\right)^{1/2}\right]^2 + \frac{U_L A_L}{2 U_H A_H}\left[\left(\frac{T_{L1}}{T_H}\right)^{1/2} - \left(\frac{T_L}{T_H}\right)^{1/2}\right]^2. \quad (40)$$

Maximizing this with respect to T_{L1}/T_H we find:

$$\left(\frac{T_{L1}}{T_H}\right)_{opt}^{1/2} = \frac{2U_H A_H + U_L A_L (T_L/T_H)^{1/2}}{2U_H A_H + U_L A_L} \quad (41)$$

and

$$W_1 + W_2 = \left(\frac{2}{U_L A_L} + \frac{1}{U_H A_H}\right)^{-1} T_H \left[1 - \left(\frac{T_L}{T_H}\right)^{1/2}\right]^2. \quad (42)$$

Finally, we maximize $W_1 + W_2$ with respect to $U_L A_L / UA$ while noting that the constraint (36) now reads $UA = U_H A_H + 2U_L A_L$. The result is:

$$(U_L A_L)_{opt} = \tfrac{1}{3} UA \quad (43)$$

which means that the UA inventory must be divided equally between $U_H A_H$, $U_M A_M$ and $U_L A_L$. The maximum combined power output is:

$$W_1 + W_2 = \tfrac{1}{9} UA T_H \left[1 - \left(\frac{T_L}{T_H}\right)^{1/2}\right]^2. \quad (44)$$

The conclusion that UA must be divided equally between all the heat exchangers is not too surprising, because when there are only two heat exchangers [Fig. 9(a)] the same UA allocation rule applies. Surprising is that the efficiency of the combined-cycle optimized in equation (44),

$$\eta = \frac{W_1 + W_2}{Q_H} = 1 - \left(\frac{T_L}{T_H}\right)^{1/2} \quad (45)$$

is the same as the efficiency of the original power plant of Fig. 9(a). Rubin and Andresen [20] had found the same efficiency formula. Equation (45) is surprising, because one of the main reasons for the development of combined-cycle power plants is the desire to increase the energy conversion efficiency (e.g. ref. [2], pp. 450–454). In conclusion, when the total heat exchange inventory is fixed and the design is optimized for maximum power, the Novikov–Curzon–Ahlborn efficiency characterizes both plants, Fig. 9(a) and (b).

Another interesting result is that the maximum power output of the combined-cycle plant, equation (44), is considerably smaller than the corresponding value of the single-cycle power plant of Fig. 9(a) (e.g. ref. [2], p. 410):

$$W = \tfrac{1}{4} UA T_H \left[1 - \left(\frac{T_L}{T_H}\right)^{1/2}\right]^2. \quad (46)$$

The ratio between equations (44) and (46) is 4/9, which is a new result. To understand it, we note that when we switch from Fig. 9(a) to Fig. 9(b) and hold UA constant, the allocation of one-third of UA to the new heat exchanger ($U_M A_M$) means that we must reduce $U_H A_H$ and $U_L A_L$. This in turn leads to a smaller heat input for the power plant of Fig. 9(b). Another reason is that in Fig. 9(a) the inner compartment is reversible, while in Fig. 9(b) that compartment contains the irreversibility due to the middle heat exchanger $U_M A_M$.

8. POWER PLANT AS AN INSULATION BETWEEN ITS HEAT SOURCE AND THE AMBIENT

In this section we reconsider the maximization of the power output in a plant with direct heat leak to the ambient, Fig. 5. We focus exclusively on the irreversibility associated with the by-pass heat leak Q_i, and assume that the irreversibilities of the two heat exchangers are negligible (note that this is the reverse of the assumption made in Section 5). The resulting power plant model is shown in Fig. 10(a). The power plant has two compartments, the by-pass thermal conductance from T_H to T_L, and the rest of the plant (the actual cycle), which is irreversibility free. The total heat input to the power plant, Q_H, is divided between the power producing compartment, Q_{eH}, and the leaky insulation, Q_{iH}.

The question, again, is under what conditions is the total power output W maximum? Consider first the heat leak through the insulation, and the physical constraint that the insulation thickness (L_i), cross-section (A_i), and effective thermal conductivity (k_i) are fixed. If, as in the model of Fig. 5, the heat leak Q_i is conserved from T_H to T_L, then the internal conductance C_i mentioned in Section 4 is simply $C_i = k_i A_i / L_i$. In general, however, the heat leak may vary across the insulation, $Q_i = Q_i(T)$, because some of the heat leak may be intercepted (and used) by the reversible power cycle (see ref. [1], Chap. 9). This possibility is illustrated in the detail of Fig. 10(b).

The total power that the reversible compartment can extract from the insulation is:

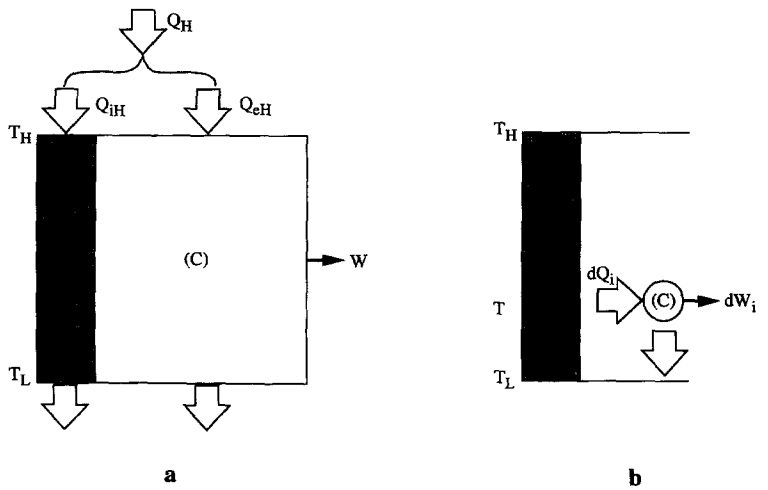

Fig. 10. (a) Power plant with by-pass heat leak to the ambient. (b) The extraction of power from the heat that flows through the internal conductance.

$$W_i = \int_{T_L}^{T_H} dW_i = \int_{T_L}^{T_H} \left(1 - \frac{T_L}{T}\right) dQ_i. \tag{47}$$

At every intermediate temperature level T the heat leak is driven by the local temperature gradient,

$$Q_i = k_i A_i \frac{dT}{dx} \tag{48}$$

where x is the position in the insulation, $x = 0$ at $T = T_L$, and $x = L_i$ at $T = T_H$. Equation (48) can be integrated across the insulation, to obtain the physical constraint:

$$\frac{L_i}{k_i A_i} = \int_{T_L}^{T_H} \frac{dT}{Q_i} \quad (\text{constant}, C_i^{-1}) \tag{49}$$

where it is assumed that k_i is temperature independent. The problem consists of finding the function $Q_i(T)$ that maximizes the W_i integral (47) subject to the integral constraint (49). The solution is readily available by variational calculus (e.g. ref. [2], p. 722): therefore we list only the results for the optimal heat leak function and the maximum W_i,

$$Q_{i,opt} = C_i \ln\left(\frac{T_H}{T_L}\right) T \tag{50}$$

$$W_{im} = C_i \ln\left(\frac{T_H}{T_L}\right)\left[T_H - T_L - T_L \ln\left(\frac{T_H}{T_L}\right)\right]. \tag{51}$$

Equation (51) represents the maximum power that can be extracted from the insulation, i.e. from the internal conductance C_i. At this stage, it is instructive to compare the maximum power W_{im} to the heat leak received by C_i from T_H, namely $Q_{iH,opt} = C_i \ln(T_H/T_L)T_H$. The ratio of these quantities is the efficiency of C_i at maximum power,

$$\eta_i = \frac{W_{im}}{Q_{iH,opt}} = 1 - \frac{T_L}{T_H} + \frac{T_L}{T_H} \ln\left(\frac{T_L}{T_H}\right) \tag{52}$$

which has been plotted as $1-\eta_i$ vs T_L/T_H in Fig. 11. This is an important plot because it shows that η_i is comparable with the maximum power efficiency derived by Novikov and Curzon and Ahlborn for the model of Fig. 9(a), namely equation (45). The dashed line is the Carnot efficiency $1-\eta = T_L/T_H$. It was shown in ref. [3], and in an expanded way in ref. [2], that equation (45) agrees approximately with the reported efficiencies of power plants in operation. The ten points plotted in Fig. 11 reproduce the reported efficiencies compiled in ref. [2]. The figure shows that equation (52) also agrees with the reported data.

What we have achieved in this section is a new thermodynamic interpretation of the design and operation of actual power plants. The agreement between equation (52) and reported data suggests that an actual power plant may be viewed as an obstacle to the direct heat transfer from the source T_H to the sink T_L, i.e. an 'insulation' designed to produce maximum power when its overall size (C_i) is constrained. Indeed, a power plant acts as an insulation between its heat source and heat sink in the same way that a refrigeration plant insulates its coldest compartment from the ambient.

9. POWER PLANT WITH BY-PASS HEAT LEAK TO THE AMBIENT

We can now return to the model of Fig. 10(a), in which the internal conductance C_i is in parallel with a reversible cycle. Let us assume that the conductance C_i has been optimized according to equations (50), (51) and Fig. 10(b). This means that in addition to W_{im} listed in equation (51), the power plant delivers the power $W_e = Q_{eH}(1 - T_L/T_H)$, where $Q_{eH} = Q_H - Q_{iH,opt}$. The total power output ($W = W_{im} + W_e$) can be nondimensionalized as an overall efficiency ratio,

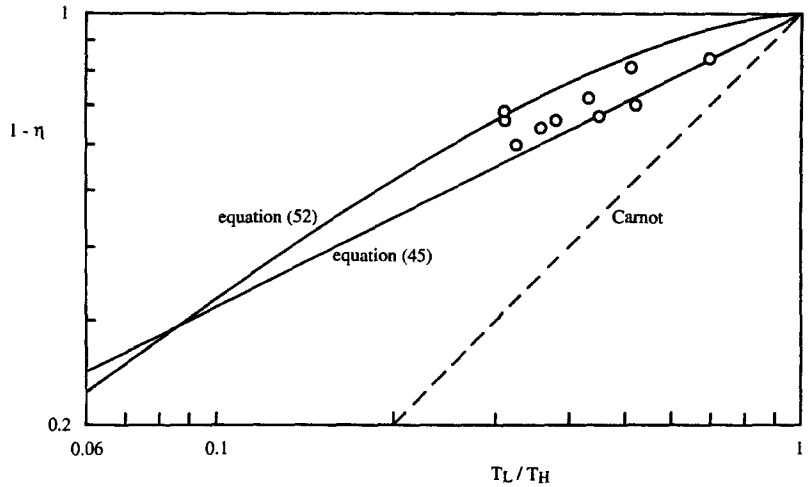

Fig. 11. The maximum-power efficiency of a power plant viewed as an insulation between its heat source and heat sink, equation (52).

$$\frac{W}{Q_H} = \tilde{C}_i \ln\left(\frac{T_H}{T_L}\right)\left[\frac{T_H}{T_L} - 1 - \ln\left(\frac{T_H}{T_L}\right)\right] + \left[1 - \tilde{C}_i \frac{T_H}{T_L} \ln\left(\frac{T_H}{T_L}\right)\right]\left(1 - \frac{T_L}{T_H}\right) \quad (53)$$

where the overall heat input Q_H is fixed, and $\tilde{C}_i$ is the nondimensional internal conductance,

$$\tilde{C}_i = \frac{C_i T_L}{Q_H}. \quad (54)$$

It can be shown numerically that the total power (53) has a maximum with respect to T_H/T_L, i.e. with respect to T_H since T_L is fixed. The power is zero in the limit $T_H = T_L$. It increases as T_H becomes greater than T_L: however, when T_H is high enough the power starts to decrease because an increasing fraction of Q_H flows through C_i. The existence of such a power maximum was noted earlier [21] (also in ref. [1], p. 44), where the heat leak was constant as it flowed through the conductance. In the present case, the heat flow through the conductance generates the maximum power of which it is capable, and the maximum W is the absolute limit that the power cycle with by-pass conductance can reach.

The numerical results are shown in Fig. 12, in which $\tilde{C}_i$ represents the size of the insulation (C_i) relative to the overall size of the plant (Q_H). For each physical configuration $\tilde{C}_i$, there is an optimal hot-end temperature $(T_H/T_L)_{opt}$, and a maximum total power out-

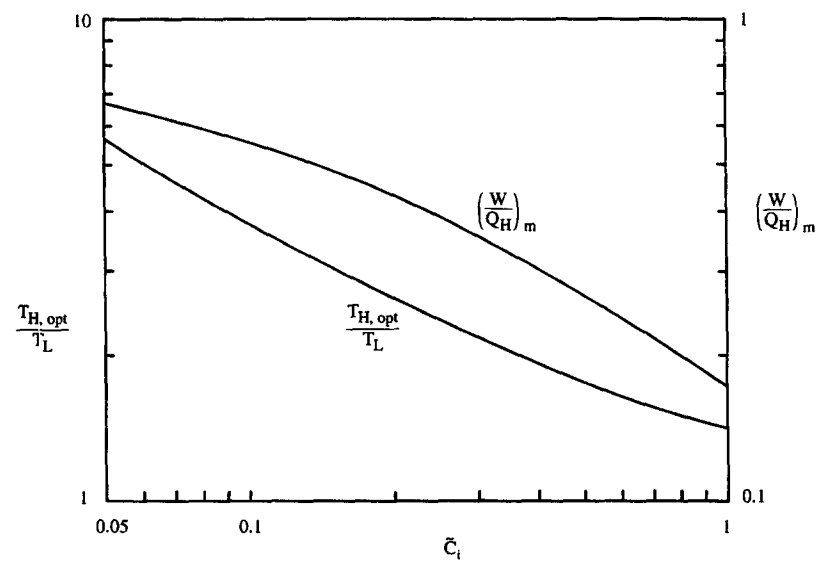

Fig. 12. The optimal hot-end temperature and the maximum power output of a plant with by-pass heat leak to the ambient [Fig. 10(a)].

put $(W/Q_H)_m$. The heat source temperature and the maximum power decrease as the relative size of the internal conductance increases.

10. CONCLUDING REMARKS

In this paper, a sequence of eight problems (Sections 2–9) were presented in which various installations with heat transfer irreversibilities were optimized by arranging the heat transfer hardware. The basic assumption was that the overall inventory of heat transfer hardware is constrained (e.g. total area A, thermal conductance UA, internal conductance C_i). The results were discussed individually at the end of each problem.

The general conclusion that unites these results is that the power output of a power plant can be maximized by dividing the finite supply of heat transfer equipment among the heat transfer components involved. At the fundamental level, this represents a step beyond what is currently done with the method of entropy generation minimization or finite-time thermodynamics. The engineering implications of this step are that if the hardware inventory can be allocated optimally in simple models such as Figs. 1, 2, 5, 9 and 10, then there is an opportunity to distribute the hardware optimally in the design of actual, much more complicated, installations. *The mission of simple models and simple theories is to show the way, i.e. to uncover new opportunities for the applied work that will follow.*

REFERENCES

1. A. Bejan, *Entropy Generation through Heat and Fluid Flow*. Wiley, New York (1982).
2. A. Bejan, *Advanced Engineering Thermodynamics*. Wiley, New York (1988).
3. F. L. Curzon and B. Ahlborn, Efficiency of a Carnot engine at maximum power output, *Am. J. Phys.* **43,** 22–24 (1975).
4. B. Andresen, P. Salamon and R. S. Berry, Thermodynamics in finite time, *Phys. Today* 62–70 (September 1984).
5. I. I. Novikov, The efficiency of atomic power stations, *J. Nucl. Energy II* **7,** 125–128 (1958); translated from *Atomnaya Energiya* **3,** 409 (1957).
6. M. M. El-Wakil, *Nuclear Power Engineering*, pp. 162–165. McGraw-Hill, New York (1962).
7. M. M. El-Wakil, *Nuclear Energy Conversion*, pp. 31–35. International Textbook Company, Scranton, PA (1971).
8. A. Bejan, Theory of heat transfer-irreversible power plants, *Int. J. Heat Mass Transfer* **31,** 1211–1219 (1988).
9. A. Bejan, D. W. Kearney and F. Kreith, Second law analysis and synthesis of solar collector systems, *J. Sol. Energy Engng* **103,** 23–30 (1981).
10. J. R. Howell and R. B. Bannerot, Optimum solar collector operation for maximizing cycle work output, *Sol. Energy* **19,** 149–153 (1977).
11. M. Sokolov and D. Hershgal, Optimal coupling and feasibility of a solar powered year-round ejector air conditioner, *Sol. Energy* **50,** 507–516 (1993).
12. A. Bejan, Theory of heat transfer-irreversible refrigeration plants, *Int. J. Heat Mass Transfer* **32,** 1631–1639 (1989).
13. S. A. Klein, Design considerations for refrigeration cycles, *Int. J. Refrigeration* **15,** 181–185 (1992).
14. A. Bejan, Power and refrigeration plants for minimum heat exchanger inventory, *J. Energy Res. Tech.* **115,** 148–150 (1993).
15. M. De Lucia and A. Bejan, Thermodynamics of energy storage by melting due to conduction or natural convection, *J. Solar Energy Engng* **112,** 110–116 (1990).
16. M. De Lucia and A. Bejan, Thermodynamics of phase-change energy storage: the effects of liquid superheating during melting, and irreversibility during solidification, *J. Sol. Energy Engng* **113,** 2–10 (1991).
17. J. S. Lim, A. Bejan and J. H. Kim, Thermodynamic optimization of phase-change energy storage using two or more materials, *J. Energy Res. Tech.* **114,** 84–90 (1992).
18. H. Bjurström and B. Carlsson, An exergy analysis of sensible and latent heat storage, *Heat Recovery Syst.* **5,** 233–250 (1985).
19. G. A. Adebiyi and L. D. Russell, A second law analysis of phase-change thermal energy storage systems, ASME HTD **80,** 9–20 (1987).
20. M. H. Rubin and B. Andresen, Optimal staging of endoreversible engines, *J. Appl. Phys.* **53,** 1–7 (1982).
21. A. Bejan and H. M. Paynter, *Solved Problems in Thermodynamics*, Department of Mechanical Engineering, Massachusetts Institute of Technology, Cambridge, MA, Problem VII-D (1976).